Strong transport and mixing of deep water through the Southwest Indian Ridge

J. A. MACKINNON*, T. M. S. JOHNSTON AND R. PINKEL
Scripps Institution of Oceanography, La Jolla, California 92093, USA
*e-mail: jmackinn@ucsd.edu

Published online: 2 November 2008; doi:10.1038/ngeo340

The Indian Ocean harbours an important but poorly understood part of the global meridional ocean overturning circulation, which transports heat to high latitudes[1]. Understanding heat exchange in the Indian Ocean requires knowledge of the magnitudes and locations of both meridional deep-water transport and mixing, but in particular the latter is poorly constrained at present[2,3]. Here we present detailed measurements of transport and mixing in the Atlantis II fracture zone in the Southwest Indian Ridge, one of the main conduits for equatorward-flowing deep water[4,5]. We observe a northward jet of deep and bottom water extending 1,000 m vertically with a transport rate of 3×10^6 m^3 s^{-1}. Turbulent diffusivity within the jet was up to two orders of magnitude above typical deep ocean levels in our measurements. Our results quantify the flow through this narrow fracture zone to 20 to 30% of the total meridional overturning circulation in the Indian Ocean, and provide an example of elevated turbulence in a deep sheared flow that is not hydraulically controlled, in contrast to many other fracture zones[6–9].

The lower limb of the Indian Ocean meridional overturning circulation (MOC) consists of northward-flowing deep and bottom water from the North Atlantic and Weddell Sea that ultimately returns south as lighter deep and intermediate waters before continuing on a global trajectory[1]. Estimates of the total rate of overturning integrated across the basin vary widely, ranging from 4 Sv (ref. 10) to 27 Sv (ref. 5), with rates from most recent studies clustering around 10–12 Sv (refs 2,11,12). (1 Sverdrup = 10^6 m^3 s^{-1}).

A key driver of the MOC is turbulent diffusion of heat from warm surface waters to cold deep waters, supplying the potential energy that drives the circulation[13]. Quantitative understanding of elevated mixing over sloping topography and narrow passages is lacking[13]. Global models generally do not have mixing parameterizations that can simulate observations of elevated mixing over rough topography. As a result, many regional modelling studies show a considerably weaker MOC due to weak diapycnal mixing prescribed at depth[14].

The northward inflow is a combination of North Atlantic Deep Water, its modified fresher form known as Circumpolar Deep Water and Antarctic Bottom Water[15]. Here we define deep water with neutral density (γ^n) from 27.96 to 28.11 kg m^{-3} and bottom water with $\gamma^n \geq 28.11$ kg m^{-3} (refs 3,5). At least half of the deep and bottom inflow occurs in the western half of the Indian Ocean, particularly in the Crozet and Madagascar basins[2]. Hydrographic studies suggest that most of this water is constrained to flow through deep fracture zones in the Southwest Indian Ridge[4,5] (SWIR). The Atlantis II fracture zone is hypothesized to be the main passageway for Circumpolar Deep Water and Antarctic Bottom Water flow through the SWIR (refs 3–5).

The Atlantis II fracture zone is deep and narrow (Fig. 1). Sills near 4,300 m and 4,200 m at the southern and northern ends constrain the water masses that enter and exit the fracture zone. Between 33°30′ S and 32° S the average east/west bathymetric profile peaks at 2,800 m on the western ridge and 2,450 m on the eastern ridge, reaching 5,700 m in between (Fig. 2). Over this latitude range, the 3,500 m isobath widens from 16 to 23 km (Fig. 1b, black contour). The steep sidewalls have slopes of the order of 0.5 (rise/run). Two gaps in the western ridge (3,600 m near 32°15′ S and 3,500 m near 32° 26′ S) may allow exchange with Madagascar basin water.

From December 2007 to January 2008, we made detailed measurements of water transport and mixing in the Atlantis II fracture zone. Two full-depth profiles of ocean temperature, salinity and currents were taken on 3 December 2007 with a further 21 profiles from 12 to 25 January. Results presented here will refer to the second set of measurements unless otherwise indicated. Of these 21 profiles, 12 were taken over 56 h at station C in the centre of the fracture zone, and zonal sections of 4 and 5 profiles were taken across the southern (S) and northern (N) end of the fracture zone (Fig. 1b).

A persistent jet of northward flow was observed at station C (Fig. 3a). The jet was centred near 3,500 m, just above the height of the southern sill and well above the bottom of the fracture zone (Fig. 2). The depth range of the jet (~2,500–4,000 m) encompasses both deep and bottom water (Fig. 4). Integrating typical velocities of 0.1–0.2 m s^{-1} over the depth range occupied by these water masses for each profile yields an average integrated flow of 360 m^2 s^{-1} for this time series (Fig. 1b, black arrows). Over the 56 h of measurement, flow magnitude fluctuated by $\pm$58 m^2 s^{-1} with the best harmonic fit giving a 15 h period; yet all profiles showed a similar jet-like structure (Fig. 3a, grey). Flow also fluctuated in direction by $\pm$15° (Fig. 1b, white lines). The similarity of velocity observed at the same location during the first cruise suggests persistence of the mean flow (Fig. 3a, magenta).

Along sections S and N, the vertically integrated flow of deep and bottom water is northward at nearly all stations (Fig. 1b). Flow is stronger in the western half of the fracture zone across both sections. Along section S, there is northward flow only in the two western stations, with weak southward flow at the two eastern stations. Along section N, the fracture zone is divided into two branches by a ridge at 3,900 m near 57°3′ E, 32° S. Water in the eastern branch may not escape the fracture zone owing to the tall topography downstream. In the two middle profiles in the

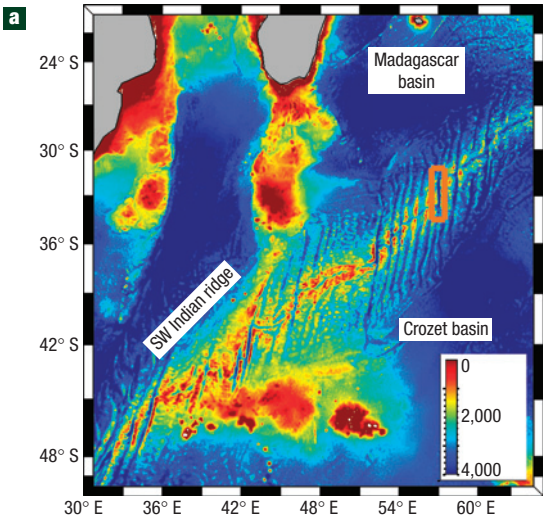

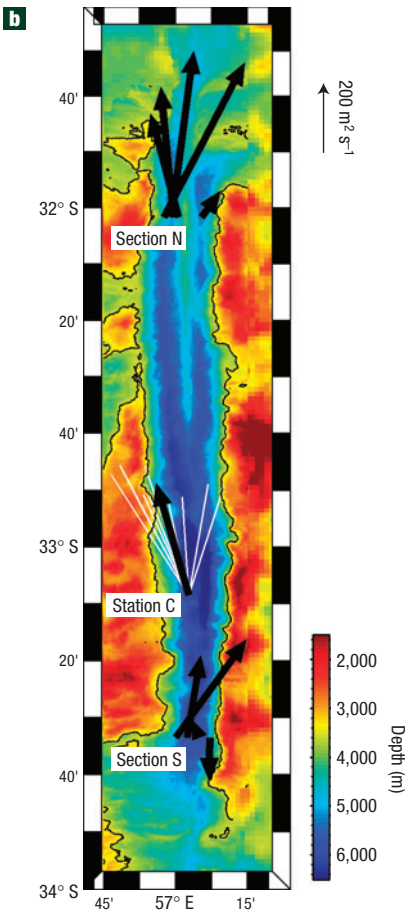

Figure 1 Transport through the southwest Indian Ocean. a, Overview map of region with bathymetric depth contoured. The study area is indicated with an orange rectangle. **b**, Expanded view of study area. Integrated flow of deep and bottom water shown with an arrow for each station; scale arrow to the right. In each case, the depth integral was conducted over the depth range defined by neutral density greater than 27.96 kg m^{-3}. The locations of the southern section (S), northern section (N) and centre station (C) are labelled. For the 12 profiles at station C, the integrated flow for each profile is shown in white and the average in black.

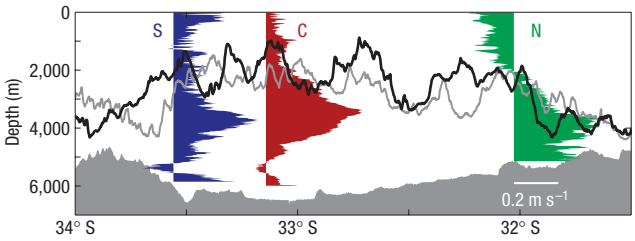

Figure 2 Jet profiles and bounding topography. The maximum depths of the fracture zone along its main axis and its western branch north of 32° 30′ S are shaded (grey), from the data in Fig. 1b. The minimum depths of the ridges to the west (grey) and east (black) are also plotted. Between the ridge crest and sills, the deep jet is found in average velocity profiles from the two western stations in section S (blue), all 2008 data at station C (red) and four western stations in section N (green). Current scale is at the lower right (white).

western branch of section N, the flow is strong and deep with velocities $>0.25\,m\,s^{-1}$ between 3,700 m and 4,700 m. Flow at the station on each edge of the western branch is weaker (peak velocity $\sim 0.15\,m\,s^{-1}$) and more diffuse (2,000–4,500 m depth).

The zonal asymmetry visible in Fig. 1b may be due to the influence of rotation[6]. Although the baroclinic Rossby radius (~22 km) barely fits across the fracture zone, the time for transport through the fracture zone in the main jet (~13 days) is significantly longer than the local inertial period, suggesting rotation has a dynamical role. However, the time aliasing of isopycnal depths due to internal-wave heaving precludes observation of dynamical balances in lateral isopycnal slopes.

The total northward transport can be estimated by interpolating between velocity profiles and integrating across both section S and the western branch of section N. Total transport for section S is 3.2 ± 1 Sv (1 Sv deep water and 2.2 Sv bottom water), whereas that for the western branch of section N is 2.9 ± 1.9 Sv (1.2 Sv of deep water and 1.9 Sv of bottom water). Measured transport is within error of hydrographic estimates taken just north of the fracture zone[4].

The observed northward deep transport in this fracture zone is a considerable fraction of the estimated 10–12 Sv of the total Indian Ocean MOC and represents one of the largest fracture-zone flows observed worldwide[7]. Once across the SWIR, the deepest waters flow westward across the southern Madagascar basin, then continue northward as a deep western boundary current along the Madagascar ridge[3]. Measured transport values in this boundary current (1.8 Sv of deep water and 1.6 Sv of bottom water) are within error of those reported here[3]. The largest source of uncertainty in our transport estimate is the short duration of measurements, which may misrepresent average transport in a system with large variability on monthly to interannual timescales. For example, stable estimates of northward transport through Hunter Channel required 200 days of measurement[16].

Turbulent diffusivity in the jet is elevated by two orders of magnitude above typical deep-ocean values (Fig. 3d). Recent estimates from global lowered acoustic Doppler current profiler (LADCP) data show an average deep diffusivity of $1–3 \times 10^{-5}\,m^2\,s^{-1}$ within 3,000 m of the bottom in the Indian and Pacific oceans and $5–10 \times 10^{-5}\,m^2\,s^{-1}$ in the North Atlantic and Southern oceans[17]. The calculated dissipation rate at station C is fairly constant across the jet (depths from 2,500–4,000 m), whereas diffusivity rises from $1 \times 10^{-4}\,m^2\,s^{-1}$ to $1 \times 10^{-2}\,m^2\,s^{-1}$ with increasing depth. Average diffusivity profiles from sections S and N are similar.

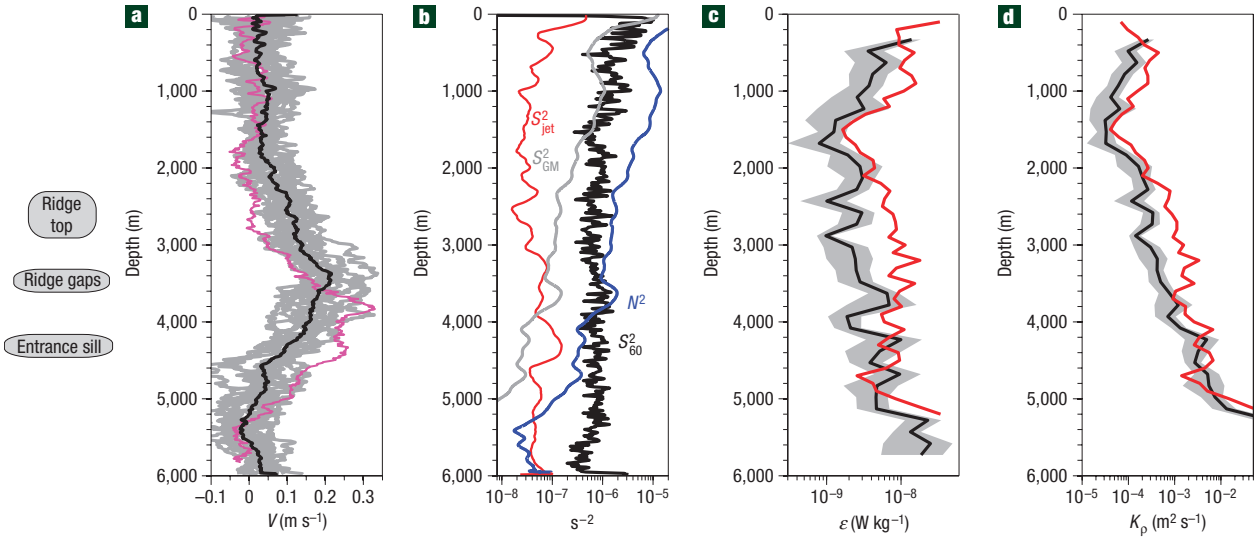

Figure 3 Vertical profiles at station C. a, Northward velocity from all of the profiles at station C (grey), their average (black) and the average of two profiles taken 3 December 2007 during a previous trip (magenta). **b**, Average buoyancy frequency profile (blue), shear variance computed from velocity smoothed to 60 m (black), shear variance computed from velocity smoothed to 700 m to represent the mean jet flow (red) and 60 m shear variance expected from the Garrett–Munk spectrum (grey). **c**, Average profiles from station C of turbulent dissipation rate calculated using shear and strain spectra (black) and Thorpe scales (red). For the former, 95% bootstrap confidence intervals are indicated with shading. **d**, Turbulent diffusivity, as in **c**.

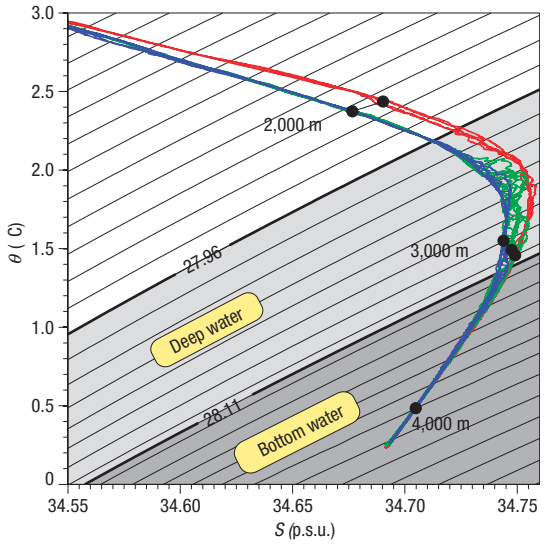

Figure 4 Changing water properties. Potential temperature (referenced to the surface) versus salinity curves showing all profiles from section S (red), station C (green) and section N (blue). The average locations of 2,000, 3,000 and 4000 m depths are labelled. Neutral density is contoured in black with labels indicating the neutral density lines used to define the upper boundaries of deep water ($\gamma^n = 27.96\,\mathrm{kg\,m^{-3}}$) and bottom water ($\gamma^n = 28.11\,\mathrm{kg\,m^{-3}}$).

The results presented here join a growing body of work arguing that strong mixing in fracture zones, submarine valleys and canyons has an important role in deep- and bottom-water modification[6–9,18–21]. In these studies, strong mixing is observed in or near regions where deep flow is hydraulically controlled (Froude number of order 1) and/or where the Richardson number ($Ri = N^2/S^2$) is of order 1 over tens to hundreds of metres vertically, suggesting the mean flow is susceptible to shear instability. However, our results show elevated turbulence in a fundamentally different setting, in which the mid-fracture-zone flow is not hydraulically controlled (Fr $\sim$ 0.1) and the mean flow shear is stable (Fig. 3b, red).

Instead, the strong mixing in the Atlantis II fracture zone may be the result of an energetic small-scale internal gravity wave field interacting with the mean flow. In the upper 1,500 m, 60 m shear variance is comparable to that of the open ocean (predicted by the canonical Garrett–Munk internal-wave spectrum[22]). Both mirror the stratification (Fig. 3b, black and grey). Below 2,000 m (in the jet), the observed 60 m shear variance diverges from Garrett–Munk values. Below 3,000 m, S^2 exceeds N^2, which may lead to strong shear instabilities. Internal tides with vertical wavelengths of the order of 100 m were observed to radiate from the steep SWIR topography. Although the mean shear is not itself unstable, internal tides or other ambient internal waves with vertical wavelengths up to hundreds of metres may refract in the mean jet shear, perhaps encountering critical layers where they completely stall and break[23], dissipating their energy as turbulence over a wide depth range. More detailed time-series measurements would be needed to verify this conjecture.

Water properties show evidence of significant mixing in the fracture zone. The deep salinity peak characteristic of Circumpolar Deep Water has noticeably eroded from section S to N (Fig. 4), suggestive of mixing with fresher water above and below. Using a transit time of 13 days, the observed change in salinity requires stronger diapycnal mixing (an average $K_\rho > 1 \times 10^{-2}\,\mathrm{m^2\,s^{-1}}$ below 2,000 m) than observed at station C. The discrepancy may be resolved if (1) mixing elsewhere in the fracture zone is stronger than observed with these limited measurements, or (2) the water has a residence time significantly longer than 13 days owing to undocumented recirculation patterns or temporal variability of the jet. A more likely explanation is isopyncal mixing with fresher Madagascar basin water, either southward along the fracture-zone axis or through gaps in the ridge. The large temperature–salinity variability as water flows past station C (Fig. 4, green) is consistent with active isopycnal stirring.

The short residence time and narrow extent of the fracture zone limit the deep diapycnal flux (0.002 Sv across $\gamma^n = 28.11\,\mathrm{kg\,m^{-3}}$), despite the large turbulent diapycnal diffusivity. However, the observed elevated turbulence in the jet provides a dynamical example of elevated turbulence in a low-Froude-number regime that may be extrapolated to flow through other fracture zones in the SWIR and to regions of deep sheared flow worldwide. Furthermore, strong mixing in the Atlantis II fracture zone is consistent with the recent argument that the observed Indian Ocean MOC requires a large zonal asymmetry in deep mixing rates, with larger diapycnal mixing over the rough topography of the western basin[24].

METHODS

DATA

Density was computed from temperature and salinity measured by the shipboard conductivity–temperature–depth package on the R/V *Roger Revelle*. Velocity at each depth was measured with a 300 kHz RDI Workhorse LADCP attached to the rosette. Each full-depth velocity profile was calculated with the inverse method of Visbeck[25] (ftp://ftp.ldeo.columbia.edu/pub/LADCP, Version IX) constrained by inclusion of shipboard navigational data, shipboard Doppler sonar measurements of velocity in the upper 1,000 m and bottom tracking by the LADCP. Spectral analysis suggests instrument noise dominates motions at wavelengths less than 50 m, with an r.m.s. noise velocity of $0.02\,\mathrm{m\,s^{-1}}$. Multibeam bathymetry for the fracture zone has a horizontal resolution of 150 m.

FLOW PROPERTIES

The baroclinic Rossby radius, $\overline{N}H/f$, can be estimated for the jet at station C using the average buoyancy frequency between 2,600 and 4,200 m ($\overline{N} = .001\,\mathrm{s^{-1}}$) and a scale height of $H = 1{,}600$ m.

The Froude number for a stratified flow can be expressed as $Fr = \overline{U}/\overline{N}H$, where we take $\overline{U}$ as the mean northward velocity at station C between 2,600 and 4,200 m; $\overline{N}$ is the average buoyancy frequency and H is the jet height[21].

Using an average jet speed of $0.15\,\mathrm{m\,s^{-1}}$ (averaged between 2,600 and 4,200 m at station C), a water parcel would take 13 days to transit between sections S and N.

NET TRANSPORT

Deep- and bottom-water masses are defined using neutral density[26]. The integrated flow for each profile was calculated by vertically integrating northward velocity over a depth range with $\gamma^n \geq 27.96\,\mathrm{kg\,m^{-3}}$. Net transport across each section was calculated by interpolating velocity between stations and integrating over the cross-sectional area of each section as given by multibeam bathymetry. Estimated error in net transport across each section is conservatively based on r.m.s. variability of northward velocity at the station C time series, which has an average of $0.076\,\mathrm{m\,s^{-1}}$ for each depth in the deep- and bottom-water ranges. Projecting this uncertainty onto the net transport calculations produces an estimated error of 1 Sv for the northern section and 1.9 Sv for the southern section. If uncertainty is instead calculated by the r.m.s. of integrated deep- and bottom-water transport at station C, transport errors drop to ± 0.3 Sv.

MIXING ESTIMATES

Estimates of diapyncal diffusivity are computed from shear and strain spectra[17]. Shear spectra were computed in half-overlapping 300 m vertical windows, and integrated out to a wavenumber cutoff of $0.1\,\mathrm{m^{-1}}$, chosen to be the wavenumber beyond which instrument noise overwhelms the signal. Strain spectra are integrated to a similar wavenumber. Diffusivity was computed in each vertical bin for each profile and then averaged. Results are similar if spectra are averaged between profiles before computing diffusivity. Dissipation rate estimates were also computed using Thorpe scale analysis of conductivity–temperature–depth density profiles[27] using run length and overturn size criteria[28]. Unresolved low dissipation levels were accounted for by using a dissipation rate of $10^{-11}\,\mathrm{W\,kg^{-1}}$ where no overturns were detected. Although the two methods generally agree well, the Thorpe scale estimate is larger by an average factor of 3 between 2,000 and 4,000 m. Previous studies have argued that the spectral method may be an underestimate in times of energetic breaking waves[29] or weak stratification[28]. Turbulent diffusivity (K_ρ) and dissipation (ϵ) are connected[30] through $K_\rho \leq 0.2\epsilon/N^2$. Diffusivity estimates in extremely weak stratification (below 5,000 m) are questionably reliable and are not plotted in Fig. 3d. The diffusivity required to explain the observed reduction in the deep salinity maximum between section S and section N was computed by applying $\Delta S(z)/\Delta t = \kappa\,\delta_{zz}\overline{S(z)}$, where ΔS is the observed decrease in the salinity maximum, $\Delta t = 13$ days, and $\overline{S(z)}$ is the average salinity profile from the southern section. A rough estimate of net diapycnal flux across the $28.11\,\mathrm{kg\,m^{-3}}$ neutral density surface was calculated in two steps. Diapycnal velocity was computed from $w_*\,\partial_z\rho = \kappa\,\partial_z^2\rho$ based on the average density profile at station C. The diapycnal velocity at the average depth of the $28.11\,\mathrm{kg\,m^{-3}}$ neutral density surface at station C ($5\times10^{-7}\,\mathrm{m\,s^{-1}}$) was integrated over the average area of this isobar from 33.5° S to 32° S using multibeam bathymetry.

Received 20 June 2008; accepted 29 September 2008; published 2 November 2008.

References

1. Ganachaud, A. & Wunsch, C. Improved estimates of global ocean circulation, heat transport and mixing from hydrographic data. *Nature* **408**, 453–457 (2000).
2. Ganachaud, A., Wunsch, C., Marotzke, J. & Toole, J. Meridional overturning and large-scale circulation of the Indian Ocean. *J. Geophys. Res.* **105**, 26117–26134 (2000).
3. Donohue, K. & Toole, J. A near-synoptic survey of the Southwest Indian Ocean. *Deep-Sea Res. II* **50**, 1893–1931 (2003).
4. Warren, B. A. Bottom water transport through the Southwest Indian Ridge. *Deep-Sea Res.* **25**, 315–321 (1978).
5. Toole, J. M. & Warren, B. A hydrographic section across the subtropical South Indian Ocean. *Deep-Sea Res. I* **40**, 1973–2019 (1993).
6. Thurnherr, A. M. *et al.* Hydrography and flow in the Lucky Strike segment of the Mid-Atlantic Ridge. *J. Mar. Res.* (2008, in the press).
7. Polzin, K. L., Speer, K. G., Toole, J. M. & Schmitt, R. W. Intense mixing of Antarctic Bottom Water in the equatorial Atlantic Ocean. *Nature* **380**, 54–57 (1996).
8. Hogg, N., Biscaye, P., Gardner, W. & Schmitz, W. J. Jr. On the transport and modification of Antarctic bottom water in the Vema Channel. *J. Mar. Res.* **40**, 231–263 (1982).
9. Ferron, B., Mercier, H., Speer, K., Gargett, A. & Polzin, K Mixing in the Romanche Fracture Zone. *J. Phys. Oceanogr.* **28**, 1929–1945 (1998).
10. Fu, L. L. Mass, heat and freshwater fluxes in the South Indian Ocean. *J. Phys. Oceanogr.* **16**, 1683–1693 (1986).
11. Robbins, P. E. & Toole, J. M. The dissolved silica budget as a constraint on the meridional overturning circulation of the Indian Ocean. *Deep-Sea Res. I* **44**, 879–906 (1997).
12. Bryden, H. L. & Beal, L. M. Role of the Agulhas Current in Indian Ocean circulation and associated heat and freshwater fluxes. *Deep-Sea Res. I* **48**, 1821–1845 (2001).
13. Wunsch, C. & Ferrari, R. Vertical mixing, energy and the general circulation of the oceans. *Annu. Rev. Fluid Mech.* **36**, 281–412 (2004).
14. Palmer, M. D., Garabato, A. C. N., Stark, J. D., Hirschi, J. J.-M. & Marotzke, J. The influence of diapycnal mixing on quasi-steady overturning states in the Indian Ocean. *J. Phys. Oceanogr.* **37**, 2290–2304 (2007).
15. van Aken, H. M., Ridderinkhof, H. & de Ruijter, W. P. M. North Atlantic deep water in the south-western Indian Ocean. *Deep-Sea Res. I* **51**, 755–776 (2004).
16. Zenk, W., Seidler, G., Lenz, B. & Hogg, N. G. Antarctic Bottom Water Flow through the Hunter Channel. *J. Phys. Oceanogr.* **29**, 2785–2801 (1999).
17. Kunze, E., Firing, E., Hummon, J. M., Chereskin, T. K. & Thurnherr, A. M. Global abyssal mixing inferred from lowered ADCP shear and CTD strain profiles. *J. Phys. Oceanogr.* **36**, 1553–1576 (2006).
18. Bryden, H. L. & Nurser, A. J. G. Effects of strait mixing on ocean stratification. *J. Phys. Oceanogr.* **33**, 1870–1872 (2003).
19. Thurnherr, A. M., St Laurent, L., Speer, K., Toole, J. & Ledwell, J. Mixing associated with sills in a canyon in the midocean ridge flank. *J. Phys. Oceanogr.* **35**, 1370–1381 (2005).
20. Thurnherr, A. M. Diapycnal mixing associated with an overflow in a deep submarine canyon. *Deep-Sea Res. II* **53**, 194–206 (2006).
21. St Laurent, L. C. & Thurnherr, A. M. Intense mixing of lower thermocline water on the crest of the Mid-Atlantic Ridge. *Nature* **448**, 680–683 (2007).
22. Gregg, M. C. & Kunze, E. Shear and strain in Santa Monica Basin. *J. Geophys. Res.* **96**, 16709–16719 (1991).
23. Muench, J. & Kunze, E. Internal wave interactions with equatorial deep jets. Part I: Momentum-flux divergences. *J. Phys. Oceanogr.* **29**, 1453–1467 (1999).
24. Drijfhout, S. S. & Garabato, A. C. N. The zonal dimension of the Indian Ocean meridional overturning circulation. *J. Phys. Oceanogr.* **38**, 359–379 (2008).
25. Visbeck, M. Deep velocity profiling using lowered acoustic doppler current profilers: Bottom track and inverse solutions. *J. Atmos. Oceanogr. Tech.* **19**, 794–807 (2002).
26. Jackett, D. & McDougall, T. A neutral density variable for the world's oceans. *J. Phys. Oceanogr.* **27**, 237–263 (1997).
27. Dillon, T. M. Vertical overturns: A comparison of Thorpe and Ozmidov length scales. *J. Geophys. Res.* **87**, 9601–9613 (1982).
28. Finnigan, T., Luther, D. & Lukas, R. Observations of enhanced diapycnal mixing near the Hawaiian Ridge. *J. Phys. Oceanogr.* **32**, 2988–3002 (2002).
29. Klymak, J. M., Pinkel, R. & Rainville, L. Direct breaking of the internal tide near topography: Kaena Ridge, Hawaii. *J. Phys. Oceanogr.* **38**, 380–399 (2008).
30. Osborn, T. R. Estimates of the local rate of vertical diffusion from dissipation measurements. *J. Phys. Oceanogr.* **10**, 83–89 (1980).

Acknowledgements

We are greatly indebted to the expertise, helpful attitude and hard work of R/V *Revelle's* captain, D. Murline, and crew. We thank K. Speer and P. Lazarevich for the generous loan of their ADCP. The work could not have been completed without the hard work of T. Aja, G. Carter, M. Goldin, T. Hughen, T. Huussen, D. Lucas, S. Nguyen and O. Sun. High-resolution bathymetry near the SWIR was obtained from multibeam instruments and provided by A. Scheirer at USGS. This work was supported by NSF grant OCE-0726783 and the University of California Ship Funds program.

Author information

Reprints and permissions information is available online at http://npg.nature.com/reprintsandpermissions. Correspondence and requests for materials should be addressed to J.A.M.